Science and Technology of Advanced Materials

ISSN: 1468-6996 (Print) 1878-5514 (Online) Journal homepage: www.tandfonline.com/journals/tsta20

Poly(ARTEMA), a novel artesunate-based polymer induces ferroptosis in breast cancer cells

Natsumi Ito, Ahmed Nabil, Koichiro Uto & Mitsuhiro Ebara

To cite this article: Natsumi Ito, Ahmed Nabil, Koichiro Uto & Mitsuhiro Ebara (2025) Poly(ARTEMA), a novel artesunate-based polymer induces ferroptosis in breast cancer cells, Science and Technology of Advanced Materials, 26:1, 2482514, DOI: 10.1080/14686996.2025.2482514

To link to this article: https://doi.org/10.1080/14686996.2025.2482514

SCIENCE AND TECHNOLOGY OF ADVANCED MATERIALS
2025, VOL. 26, NO. 1, 2482514
https://doi.org/10.1080/14686996.2025.2482514

Taylor & Francis
Taylor & Francis Group

FOCUS ISSUE ARTICLE

OPEN ACCESS Check for updates

Poly(ARTEMA), a novel artesunate-based polymer induces ferroptosis in breast cancer cells

Natsumi Ito[a,b], Ahmed Nabil[a], Koichiro Uto[a] and Mitsuhiro Ebara[a,b,c]

[a]Research Center for Macromolecules and Biomaterials, National Institute for Materials Science (NIMS), Tsukuba, Japan;
[b]Graduate School of Pure and Applied Sciences, University of Tsukuba, Tsukuba, Japan;
[c]Graduate School of Advanced Engineering, Department of Materials Science and Technology, Tokyo University of Science, Katsushika-ku, Japan

ABSTRACT

Ferroptosis, a form of non-apoptotic cell death, is emerging as a promising strategy for cancer therapy. Artesunate (ART), an extract obtained from the traditional Chinese medicine Qinghaosu, has been shown to exhibit anti-cancer activity by inducing ferroptosis in cancer cells. While previous research has focused on incorporating ART monomer into drug delivery systems for enhanced cancer targeting, this study presents 2-methacryloyloxyethyl ART polymer (poly(ARTEMA)), a novel polymer synthesized from ART for the first time. Our goal was evaluation of poly(ARTEMA) anticancer potential on breast cancer cells. First, we synthesized ARTEMA using esterification followed by its polymerization using the reversible addition-fragmentation chain transfer (RAFT) polymerization method. We evaluated its mechanism of action, focusing on two key pathways: temperature-triggered singlet oxygen generation and ferrous ions (Fe^{2+}) release, both of which contribute to ferroptosis. Our results demonstrate that poly(ARTEMA) selectively generates singlet oxygen and Fe^{2+} due to the endoperoxide crosslinks, leading to cell death in breast cancer cells. We also investigated the anti-cancer potential of poly(ARTEMA) on breast cancer cells with and without a ferroptosis inhibitor. The IC_{50} values were 125 μM for the MCF-7 cancer cell line and 300 μM for the normal MCF-10 cell line, indicating enhanced toxicity toward cancer cell lines. These findings suggested that poly(ARTEMA) induces ferroptosis in cancer cells and may serve as a promising candidate for cancer therapy with minimal cytotoxicity. To the best of our knowledge, this report may be the first that successfully synthesized poly(ARTEMA) using ART, with its anticancer potential evaluation.

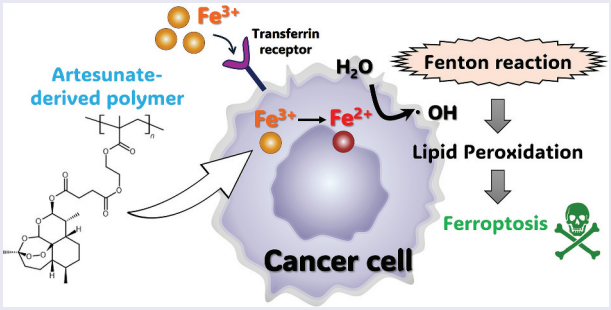

IMPACT STATEMENT

This study introduces poly(ARTEMA), a novel artesunate-based polymer for the first time that selectively induces ferroptosis in cancer cells, offering a promising strategy for non-apoptotic cancer therapies with minimal cytotoxicity.

ARTICLE HISTORY
Received 30 December 2024
Accepted 17 March 2025
Revised 26 February 2025

KEYWORDS
Cancer therapy; ferroptosis; artesunate; endoperoxide; ferrous iron; poly(ARTEMA)

1. Introduction

Despite significant advances in anti-cancer therapies, treatment failures in clinical settings remain common, resulting in poor prognosis for many cancer patients [1]. One of the factors contributing to this is the complex role of the innate immune system in the tumor microenvironment (TME), which plays a complex role in the regulation of cancer metastasis and the response to treatments [2]. Such complex effects are mediated by a network of cytokines,

CONTACT Mitsuhiro Ebara EBARA.Mitsuhiro@nims.go.jp Research Center for Macromolecules and Biomaterials, National Institute for Materials Science (NIMS), 1-1 Namiki, Tsukuba 305-0044, Japan
Supplemental data for this article can be accessed online at https://doi.org/10.1080/14686996.2025.2482514

enzymes, and iron released by innate immune cells, which interact with cancer cells through cell-cell contact [3,4]. Iron metabolism, including cancer-associated inflammation, is considered a key factor in determining the fate of cancer cells. Iron is essential for both normal and pathological cellular processes and plays a key role in cell growth and proliferation [5]. Iron is also essential for tumor initiation and progression. For example, cancer stem cells (CSCs) often express increased levels of iron-related proteins and oxidative stress, demonstrating that iron metabolism likely regulates malignancy and CSC stemness in hepatocellular carcinoma (HCC) [6,7].

Ferroptosis is a newly identified form of cell death that differs from apoptosis, necrosis, autophagy, and other types of cell death [8]. The hallmark of ferroptosis is the iron-dependent accumulation of lipid hydroperoxides [9,10]. In many cancers, intracellular iron accumulation is promoted by overexpression of transferrin receptor 1 (TFR1), a key protein responsible for iron uptake [11,12]. During this process, Fe^{2+} and hydrogen peroxide (H_2O_2) interact to generate highly reactive hydroxyl radicals (·OH), a reaction known as the Fenton reaction [13,14]. These hydroxyl radicals remove hydrogen from lipids to form a lipid radical. These lipid radicals then combine with oxygen (O_2) to produce lipid peroxyl radicals, which continue to undergo a chain reaction of oxidation reactions.

Recently, ART, a derivative of artemisinin – an extract from the traditional Chinese medicine Qinghaosu – has shown promising anti-cancer effects by inducing ferroptosis in cancer cells [15,16]. ART is widely used in the clinical treatment of malaria [17]. The endoperoxide (EP) crosslink in ART is cleaved in the presence of Fe^{2+} and triggers the Fenton reaction that generates reactive oxygen species (ROS) and lipid peroxides, ultimately leading to ferroptosis [18]. ART has gained attention because cancer cells are particularly susceptible to ferroptosis, as they often have increased iron uptake and reduced iron export mechanisms.

Despite its potential, there are several challenges in utilizing ART for cancer treatment. For instance, the total iron content in the human body is approximately 3–4 g, with about 70% (2–3 g) stored in red blood cells [19]. Additionally, significant amounts of iron are found in organs and immune cells such as macrophages. Consequently, when artesunate is administered systemically as a small-molecule drug, off-target effects may occur in iron-rich tissues other than cancer cells [20].

Another challenge is its rapid renal clearance. Artemisinin, the parent compound of ART, exhibits a peak plasma concentration within 1–2 hours and has a short half-life of approximately 2–3 hours [21]. This necessitates multiple administrations, making it unsuitable for effective cancer treatment.

To address these limitations, in the present study, we present ART-inspired polymer (poly(ARTEMA)) for the first time and characterized its therapeutic effects on breast cancer cells. We evaluated ARTEMA based on two proposed degradation pathways for its EP crosslink: singlet oxygen generation triggered by temperature and Fe^{2+} release [18,22–24]. Both singlet oxygen and Fe^{2+} have been reported to be critical factors for inducing ferroptosis. We also investigated the anti-cancer effects of ARTEMA on breast cancer cells, both with and without a ferroptosis inhibitor.

The polymerization of ART allows for extensive design versatility. In the future, adjustments to polymer size and the selection of copolymers to balance hydrophilicity and hydrophobicity could lead to designs that reduce renal clearance. Additionally, introducing receptor-specific ligands may enhance targeted delivery. Furthermore, polymer morphology can be tailored to suit different cancer types. In this study, we focused on developing poly(ARTEMA), which has the potential to overcome these challenges and expand the applicability of ART-based therapies, particularly in breast cancer treatment.

2. Materials and methods

2.1. Materials

2-Hydroxyethyl methacrylate (HEMA), 4-dimethylaminopyridine (DMAP), super dehydrated dichloromethane (anhydrous DCM), 1 mol/L sodium chloride solution (1 M NaCl), dimethyl sulfoxide-d6, 99.9%, containing 0.05 vol% tetramethylsilane (TMS) (DMSO-d6), 2,2'-Azobis(4-methoxy-2,4-dimethylvaleronitrile) (V-70), 2,2'-Azobis(isobutyronitrile) (AIBN), super dehydrated N,N-dimethylformamide (anhydrous DMF), N,N-dimethylformamide (DMF), super dehydrated dimethyl sulfoxide(anhydrous DMSO), and 1,3-diphenylisobenzofuran (DPBF) were purchased from Fujifilm Wako Pure Chemical Corporation (Osaka, Japan). ART was purchased from Tokyo Chemical Industry Co., Ltd. (Tokyo, Japan). 1-(3-Dimethylaminopropyl)-3-ethylcarbodiimide Hydrochloride (WSC) was purchased from Dojindo Laboratories Co., Ltd. (Kumamoto, Japan). 4-Cyano-4-[[(dodecylthio)carbonothioyl]thio]pentanoic acid (CDSPA) and Minimum Essential Medium Eagle (MEM) were purchased from Sigma-Aldrich (St. Louis, MI, U.S.A.). MCF-7 cells were purchased from the RIKEN Bioresource Center (Tsukuba, Japan). Fetal bovine serum (FBS) of South American origin was purchased from Biowest (Nuallie, France). Dichloromethane (DCM), penicillin – streptomycin, and Dulbecco's phosphate-buffered saline (PBS) were purchased from Nacalai Tesuque (Kyoto, Japan). MCF-10 cells were purchased from the American

Type Culture Collection (Manassas, VA, U.S.A.). MEGM™ Mammary Epithelial Cell Growth Medium BulletKit™ was purchased from Lonza Group AG (Basel, Switzerland).

2.2. Synthesis of ARTEMA

ARTEMA was synthesized using HEMA, ART, WSC as a coupling agent, and DMAP as a catalyst via the esterification method in anhydrous DCM. Monomerization was conducted in a two-neck flask at room temperature (RT) for 21 h under a nitrogen atmosphere. Subsequently, liquid-liquid extraction was performed using DCM and 1 M NaCl. The resulting DCM layer was concentrated using a rotary evaporator and dried overnight under vacuum. The structure of ARTEMA was determined using ^{1}H-NMR spectroscopy at 400 MHz (JEOL, Tokyo, Japan). All NMR samples were prepared in DMSO-d6, with all values quoted in ppm relative to TMS as an internal reference.

2.3. Synthesis of poly(ARTEMA) and comparative polymer(poly(HEMA))

Poly(ARTEMA) was synthesized via conventional RAFT polymerization in anhydrous DMF, with V-70 as the initiator and CDSPA as the chain transfer agent. Polymerization was conducted in a two-neck flask at 30°C for 21 h under a nitrogen atmosphere. After the reaction, the polymer solution was dialyzed against a Spectra/Por 7 membrane (MWCO 1000; Funakoshi Co., Ltd., Tokyo, Japan) for 24 h. The polymers were then freeze-dried to obtain poly(ARTEMA).

For comparison, poly(HEMA) was synthesized under similar conditions, except using AIBN as the initiator and a polymerization temperature of 60°C. The resulting poly(HEMA) was subjected to the same dialysis and freeze-drying procedures as poly(ARTEMA). The molecular weight of both polymers was measured using gel permeation chromatography (GPC; JASCO International, Tokyo, Japan) where the eluent was DMF with lithium bromide (LiBr, 10 mm; Tosoh Corporation, Tokyo, Japan). The structures were determined by ^{1}H-NMR.

2.4. Confirmation of endoperoxide crosslink

Based on the studies by Ding et al. [22] and Wakagi et al. [25], the sample was dissolved in anhydrous DMSO and bubbled with nitrogen for 10 min. DPBF was dissolved in anhydrous DMSO to obtain a 0.19 mm solution under light-protected conditions, which was bubbled with nitrogen for 10 min. The sample solution (100 µL/well) and the DPBF solution (100 µL/well) were added to a 96-well clear bottom plate with black frame. The plate was transferred to a heated (35°C) microplate reader (Infinite 200 PRO, Tecan, Switzerland), and absorbance was measured at 413 nm 120 times at 1-min intervals.

2.5. Cell culture

Breast cancer cell line, MCF-7 was cultured in MEM supplemented with 10% FBS and 1% penicillin-streptomycin, at 37°C in a humidified environment containing 5% CO_2. Non-tumorigenic breast epithelial cell line, MCF-10 was cultured in MEGM™ Mammary Epithelial Cell Growth Medium BulletKit™ at 37°C in a humidified environment containing 5% CO_2.

2.6. Detection of cellular singlet oxygen in vitro

To detect intracellular singlet oxygen, a Singlet Oxygen Sensor Green (SOSG; Thermo Fisher Scientific, U.S.A.) was used as previously described by Flors et al. [26]. The SOSG reagent was dissolved in methanol to obtain a 5 mM stock solution. Cells were incubated in 3.5-cm glass-bottomed dishes at an initial density of 5.0×10^5 cells/cm^2 for 7 h at 37°C and under an atmosphere with 5% CO_2. The cells were then washed twice with PBS to remove the medium. Then SOSG (final concentration 10 µM; 2 mL/dish) and different concentrations of sample solution dispersions (2 mL/dish) were added in each dish and co-incubated with cells for 30 min, respectively. Finally, the cells were washed twice with PBS to remove residual cells. Fluorescence images were captured using a fluorescence microscope (Eclipse Ti2-E microscope, Nikon Corporation, Tokyo, Japan), and fluorescence intensity was quantified from the obtained images using the image analysis software NIS-Elements.

2.7. Detection of cellular Fe^{2+} ions generated in vitro

To detect intracellular Fe^{2+}, FerroOrange™ (Dojindo Laboratories, Kumamoto, Japan) was used according to the manufacturer's instructions and the previous report by Guo et al. [27]. Cells were incubated in 3.5-cm glass-bottomed dishes at an initial density of 2.5×10^5 cells/cm^2 for 7 h at 37°C and under an atmosphere with 5% CO_2. Then the cells were washed twice with PBS to remove the medium. Different concentrations of sample dispersion (2 mL/dish) were added to each dish and co-incubated with the cells for 30 min. Then, the cells were again washed twice with PBS to remove any residual cells. Finally, FerroOrange™ (2 mL/dish) was added to each dish. Fluorescence images were captured using an Eclipse Ti2-E fluorescence microscope.

2.8. MTT[3-(4,5-dimethyl-2-thiazolyl)-2,5-diphenyltetrazolium bromide] assay

The cytotoxicity of ART and its polymers was tested using a standard MTT assay (Nacalai Tesque, Kyoto,

Japan). Cells were incubated in 96-well plates with an initial density of 3.5×10^4 cells/well for 12 h at 37°C and under an atmosphere with 5% CO_2. Different concentrations of the sample dispersions (10 µL/well) were added to each well and co-incubated with the cells for 24 h. MTT solution (10 µL/well) was added to each well followed by another 2 h incubation. Finally, the solubilization solution (100 µL/well) was added to each well followed by another 1 h incubation. The absorbance of each well was measured at 570 nm by using an Infinite 200 PRO microplate reader.

2.9. Statistical analysis

Data were expressed as means ± standard deviation, unless otherwise stated. Statistical comparison was performed using a Multiple Comparisons with Tukey's multiple comparison test using EZR (Saitama Medical Center, Jichi Medical University, Saitama, Japan), which is a graphical user interface for R (The R Foundation for Statistical Computing, Vienna, Austria). More precisely, it is a modified version of R commander designed to add statistical functions frequently used in biostatistics. A p-value of less than 0.05 was considered statistically significant [28].

3. Results and discussion

3.1. Characterization of poly(ARTEMA)

Scheme 1 illustrates the synthesis of poly(ARTEMA). To demonstrate that poly(ARTEMA) retains the effects of ART, poly(HEMA) was also synthesized as a comparison (Scheme S1). Structural analysis by ^{1}H-NMR confirmed the successful synthesis of poly (ARTEMA) and poly(HEMA) (Figure S1). Molecular weight analysis using GPC indicated that the molecular weight was well-controlled (Table 1). However, the EP crosslinks (R-O-O-R') within the polymer degrade through redox reactions involving iron [18]. Because poly(ARTEMA) was synthesized using RAFT polymerization, which involves electron transfer, there was a concern about whether the synthesis process might affect the integrity of the EP crosslinks. To address this concern, we evaluated the structural stability of the EP crosslinks, which are critical for the therapeutic efficacy of ART, using DPBF. DPBF absorbs light at 413 nm, and its absorbance diminished upon reaction with singlet oxygen. We monitored changes in DPBF absorbance to assess the influence of singlet oxygen generated by thermal degradation of EP crosslinks at 35°C. ART reduced the absorbance of DPBF in a concentration-dependent

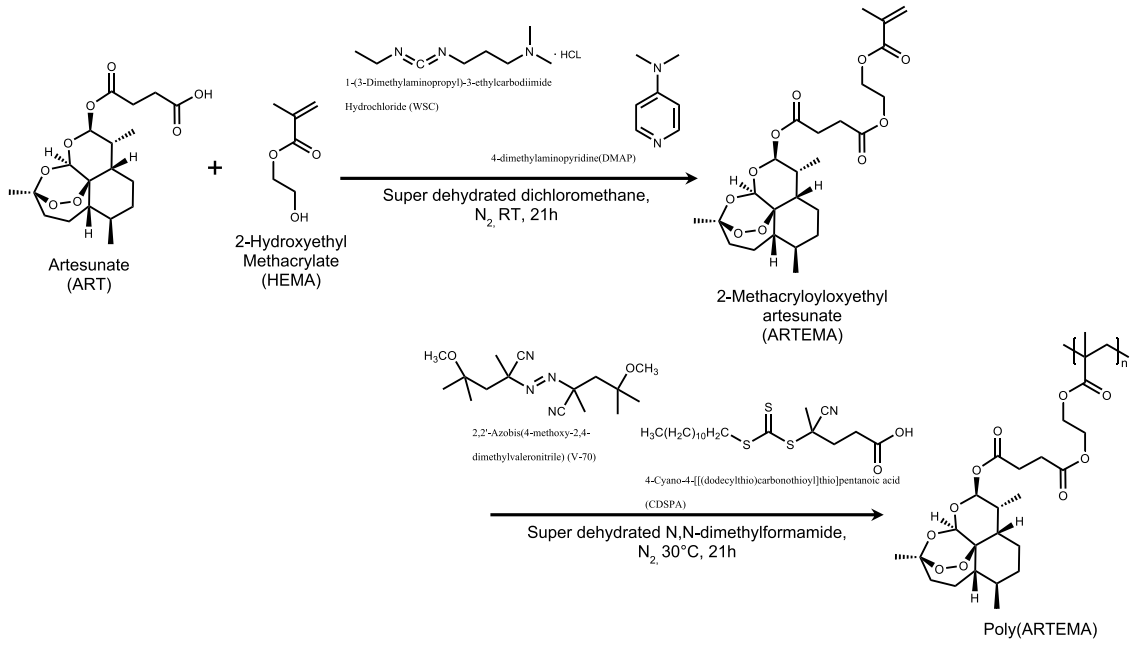

Scheme 1. Reaction scheme for the synthesis of poly(ARTEMA).

Table 1. Characterization of polymers.

Sample	Average Molecular Wight[a]		Dispersity Index[a]	
	M_n	M_w	PDI	ARTEMA (unit)[a]
Poly(ARTEMA) 4k	4.47×10^3	5.74×10^3	1.28	9
Poly(ARTEMA) 9k	9.03×10^3	9.62×10^3	1.07	18
Poly(ARTEMA) 10k	10.6×10^3	14.7×10^3	1.39	21
Poly(ARTEMA) 30k	28.7×10^3	33.7×10^3	1.18	56
Poly(HEMA)	5.88×10^3	8.05×10^3	1.37	0

[a]Calculated by GPC.

manner with respect to EP crosslinking (Figure S2). The sample concentrations were adjusted to ensure an ART monomer concentration (EP crosslink concentration) of 1.9 mM for each sample, and the results were analyzed (Figure 1). Poly(HEMA), without EP crosslinks, exhibited no significant changes in absorbance. In contrast, ART reduced absorbance, which stabilized after approximately 30 min. Poly(ARTEMA) displayed a similar trend, with absorbance changes nearly identical to those observed for ART. The degradation of EP crosslinks, indicated by changes in DPBF absorbance, is consistent with previous findings reported by Ding et al. [22] who reported that, using DPBF, the formation of ROS by the interaction of ART and Fe^{2+} is completed within 30 min. These results confirm that the synthetic process does not adversely affect the structural integrity of the EP crosslinks.

3.2. In vitro assessment of singlet oxygen

The in vivo effects of ART EP crosslinking can be attributed to multiple pathways. One proposed mechanism involves the release of singlet oxygen, a type of ROS, from the oxygen atoms of EP crosslinks in response to physiological temperatures (Figure 2, pathway 1). Previous studies have demonstrated that EP crosslinks generate singlet oxygen under physiological conditions via thermal decomposition, without radical formation [23]. The generation of singlet oxygen is thought to proceed via two mechanisms: the diradical mechanism, in which one C-O bond undergoes homolytic cleavage, and the concerted mechanism, where both C-O bonds cleave simultaneously [24]. Unlike other ROS, singlet oxygen reacts in a highly specific way with biomolecules [23,29]. Singlet oxygen produced by EP crosslinks decomposition induces oxidative stress in cells, triggering ferroptosis [23,30]. In the current study, ART and poly(ARTEMA) were incubated with MCF-7 cancer cells at 37°C for 30 min to observe the intracellular generation of singlet oxygen. Fluorescence imaging (Figure 3a) showed strong green fluorescence from SOSG in cancer cells treated with ART and poly (ARTEMA), compared to the untreated control group, where only PBS was incubated with the cancer cells. This suggests that both compounds are capable of generating singlet oxygen within cancer cells. However, quantitative analysis of the fluorescence intensity showed that poly(ARTEMA) exhibited

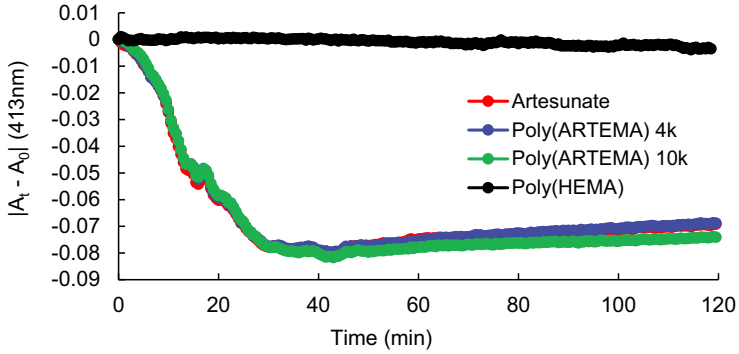

Figure 1. Change in the absorbance of 1,3-diphenylisobenzofuran (DPBF) at 413 nm during the reaction of DPBF with singlet oxygen in the presence of samples. (Sample concentration: 1.9 mM).

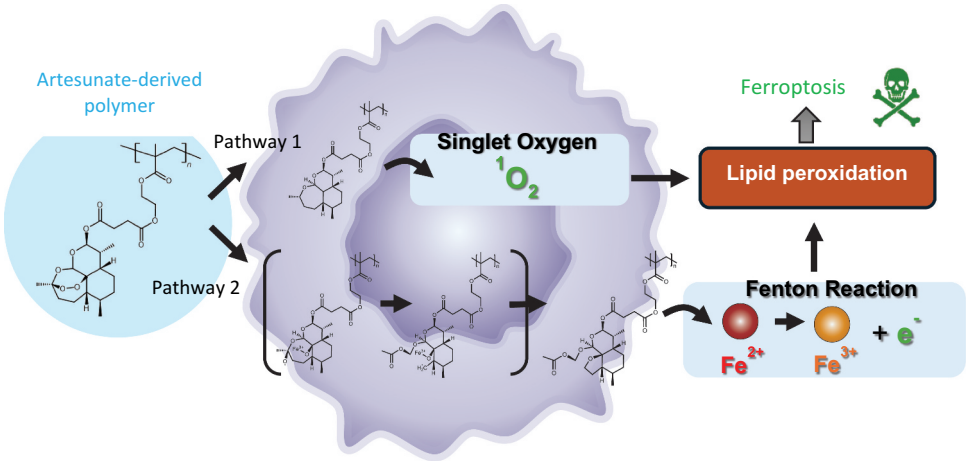

Figure 2. The underlying mechanism of the endoperoxide function of poly(ARTEMA).

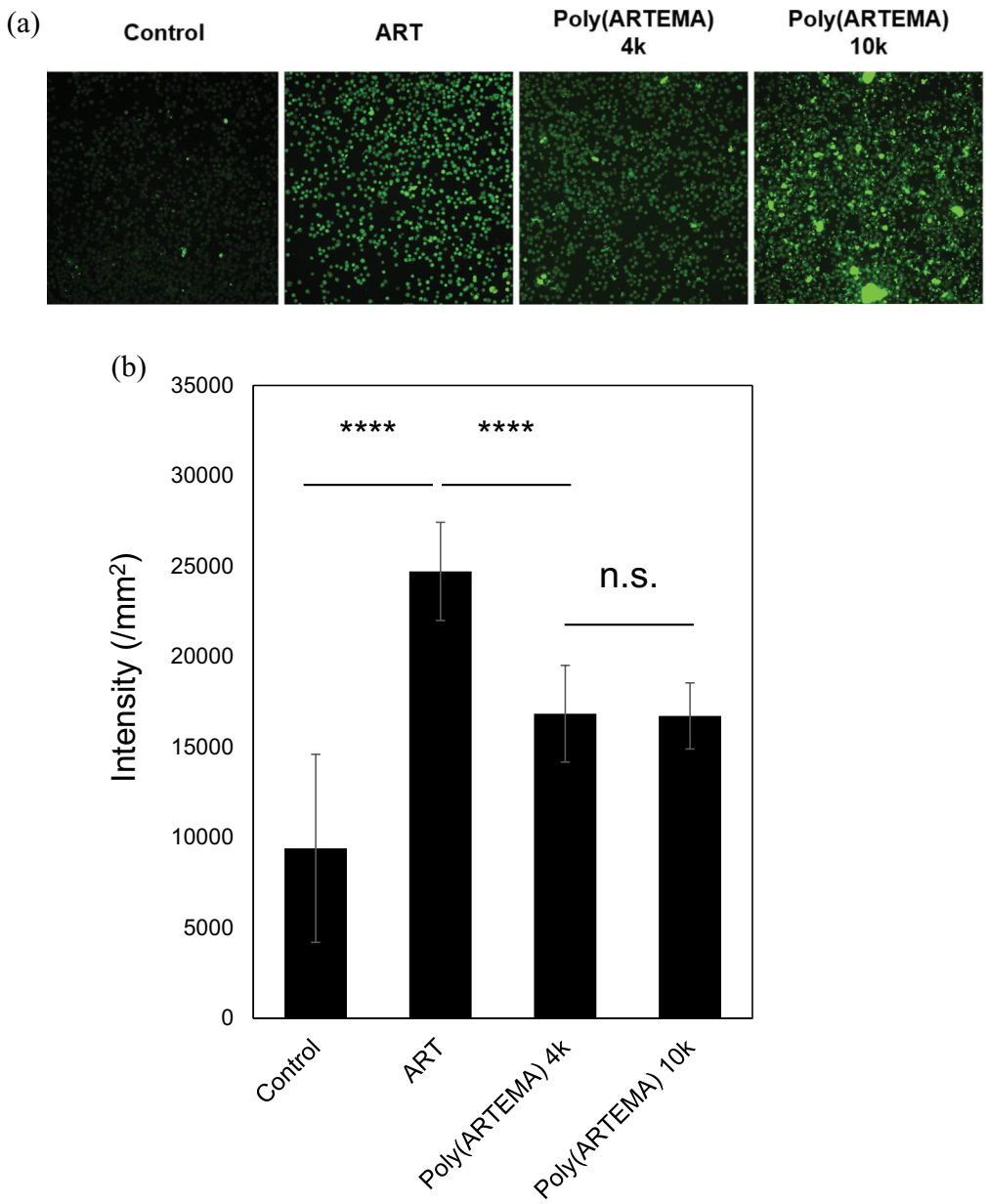

Figure 3. Fluorescence staining with singlet oxygen sensor green (SOSG). (a) Fluorescence images of MCF-7 cells treated with ART, poly(ARTEMA) 4k, and poly(ARTEMA) 10k at a concentration of 100 µm. Cell density: MCF-7 : 2.0×10^5 cells/mL. (b) Quantification of fluorescence intensity from (a) based on image analysis. Statistical significance: ****$p < 0.0001$. (mean ± SD).

a lower fluorescence intensity than ART (Figure 3b), likely due to the increased hydrophobicity of poly(ARTEMA), which led to aggregation. While HEMA is a hydrophilic monomer, it exhibits reduced water solubility upon polymerization [31]. Additionally, the ARTEMA monomer, synthesized by esterifying the hydrophilic carboxyl (–COOH) group of ART with the hydroxyl (–OH) group of HEMA, increases the hydrophobicity of the resulting polymer, potentially causing aggregation. Fluorescence imaging confirmed the formation of aggregates that emitted strong green fluorescence. Furthermore, dynamic light scattering measurements also indicated the presence of heterogeneous polymer aggregates. ART easily enters the cells and immediately generates singlet oxygen. In contrast, poly(ARTEMA) forms heterogeneous aggregates, some of which remain outside the cells. Therefore, the amount of poly(ARTEMA) directly acting within the cells was lower compared to ART, leading to a decrease in fluorescence intensity. Since this study did not employ a time-dependent measurement approach, we were unable to assess how singlet oxygen generated outside the cells by poly(ARTEMA) affects the cells or whether prolonged release of singlet oxygen is feasible. However, we believe that controlling the polymer size in future studies could provide insights into these aspects.

3.3. *In vitro assessment of Fe^{2+} ion generation*

Fe^{2+} is a critical component in the ferroptosis pathway, a process highly dependent on iron. The

presence of excessive Fe^{2+} spontaneously triggers the Fenton reaction, leading to the production of free radicals that promote lipid oxidation [32]. Like singlet oxygen, free radicals are a type of ROS with potent oxidative properties. Fe^{2+} is hypothesized to be generated through interactions between the EP crosslink and intracellular iron (Figure 1, Pathway 2) [18]. Cancer cells, such as breast cancer cells, express more transferrin receptors than normal cells and take up more iron [18,33,34]. To investigate Fe^{2+} levels, we used FerroOrange™ staining to visualize intracellular Fe^{2+} in MCF-7 cancer cells and MCF-10 normal cells (Figure 4a). Fluorescence imaging revealed that cancer cells inherently retained higher levels of Fe^{2+} than normal cells. In cancer cells, we examined the effects of ART and poly(ARTEMA) on Fe^{2+} production (Figure 4b). The addition of ART increased Fe^{2+} levels in cancer cells, as indicated by strong red fluorescence, compared to the untreated control group, where only PBS was incubated with the cancer cells. Poly(ARTEMA) showed a similar fluorescence pattern, suggesting that polymerization did not inhibit its ability to increase intracellular Fe^{2+} levels. These levels were observed 30 min after the addition of the sample, coinciding with the degradation of EP crosslinks and the generation of singlet oxygen. These results support the hypothesis that Fe^{2+} release is closely associated with the breakdown of EP crosslinks. In normal cells (MCF-10), neither ART nor poly(ARTEMA) significantly increased Fe^{2+} levels compared to cancer cells (Figure S3). These results suggest that both ART and poly(ARTEMA) selectively elevate Fe^{2+} levels in cancer cells.

3.4. Poly(ARTEMA) cancer cytotoxicity

Finally, the cytotoxicity of poly(ARTEMA) was assessed. Poly(ARTEMA) with a molecular weight of 4000 was applied to the cancer cell line MCF-7 and the normal cell line MCF-10. The IC_{50} value was determined to be 125 μM for MCF-7 and 300 μM for MCF-10 (Figure 5a). At concentrations up to 250 μM, poly(ARTEMA) caused no significant change in cell viability in MCF-10. In contrast, it exhibited strong dose-dependent cytotoxicity in MCF-7 cells. These findings suggested that poly(ARTEMA) selectively induces cytotoxicity in cancer cells.

Further, we investigated the effect of the polymer's molecular weight on cytotoxicity (Figure 5b). First, the cytotoxicity of ART was evaluated. Cell viability was compared in the presence and absence of Ferrostatin-1 (Fer-1), a known inhibitor of lipid peroxidation in the ferroptosis pathway (Figure S4) [35]. At 125 μM, ART-induced ferroptosis was significantly inhibited. Based on this result, we assessed the cytotoxicity of ART, poly(ARTEMA) 4k, poly(ARTEMA) 10k, and poly(HEMA) against MCF-7 cells at concentrations below 250 μM. Although the monomer concentration was kept constant, ensuring the EP crosslink concentration was equivalent, poly(ARTEMA) with a molecular weight of 10,000 exhibited lower cytotoxicity than the polymer with a molecular weight of 4000. These observations are consistent with previous findings from singlet oxygen measurements and are likely due to polymer aggregation [31]. Further studies are needed to explore the influence of polymer molecular weight and morphology on cellular uptake and cytotoxicity.

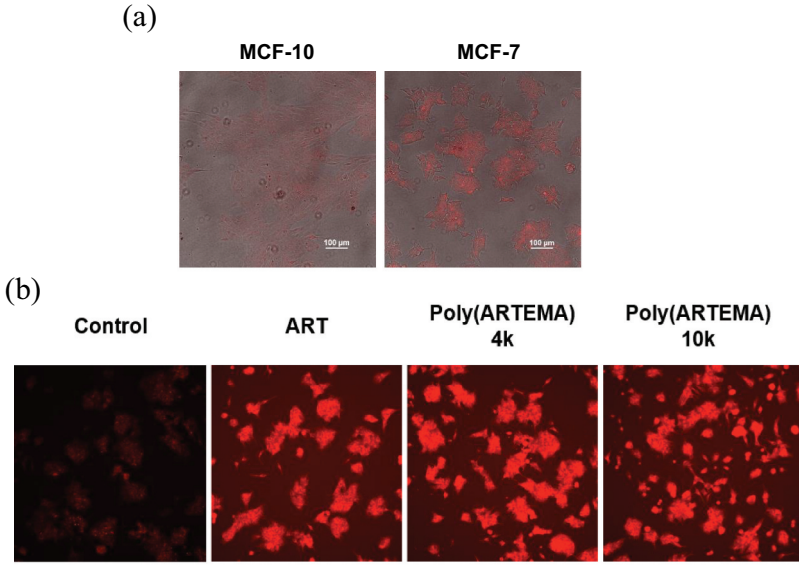

Figure 4. Fluorescence staining with FerroOrange™. Cell density: MCF-7: 1.0×10^5 cells/mL, MCF-10: 1.0×10^5 cells/mL. (a) Merged images of Fe^{2+} staining in MCF-7 and MCF-10 cells. (b) Fluorescence images of Fe^{2+} staining in MCF-7 cells treated with ART, poly(artema) 4k, and poly(artema) 10k at concentrations of 100 μm.

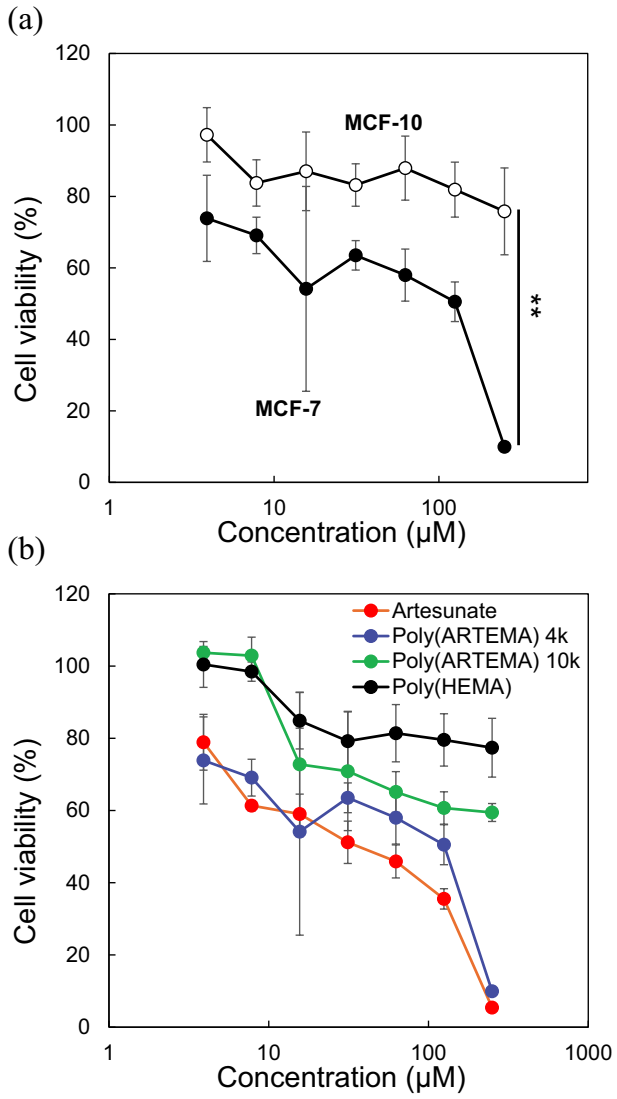

Figure 5. Cytotoxicity evaluation using the MTT assay (mean ± SD, $n = 4$). Measurements were performed at 570 nm (mode) with a reference wavelength of 670 nm. Cell density: MCF-7: 3.5×10^4 cells/well, MCF-10: 3.5×10^4 cells/well. (a) Cytotoxicity of poly(ARTEMA) 4k against MCF-7 and MCF-10 cells. $^{**}p < 0.01$. (b) Cytotoxicity of ART, poly(ARTEMA) 4k, poly(ARTEMA) 10k, and poly(HEMA) against MCF-7 cells.

4. Conclusion

Previous studies have explored the use of ART in drug delivery systems, especially to enhance its cancer-targeting ability by forming complexes with transferrin receptors. However, direct polymerization of ART has not yet been reported. Furthermore, the mechanisms of action of ART and its effects on cancer cells remain unclear. In this study, we successfully synthesized poly(ARTEMA) using ART, marking, to the best of our knowledge, the first report of this polymerization and a significant advancement in this field. We evaluated the synthesized polymer based on two proposed degradation pathways for EP crosslinking: temperature-triggered singlet oxygen generation and Fe^{2+} release. Both singlet oxygen and Fe^{2+} are known to play crucial roles in inducing ferroptosis. Our findings demonstrated that poly(ARTEMA) produces singlet oxygen and Fe^{2+}, selectively inducing cell death in cancer cells. These results suggest that poly(ARTEMA) is capable of inducing non-apoptotic cell death via ferroptosis and hold promise as a novel strategy for cancer therapy.

Disclosure statement

No potential conflict of interest was reported by the author(s).

Funding

This work was supported by the JSPS KAKENHI Grant-in-Aid for Scientific Research (B); under grant [JP19H04476]; Grant-in-Aid for Transformative Research Areas (A); under grant [JP20H05877]. This work was supported by JST, the establishment of university fellowships for the creation of science technology innovation, and Grant Number [JPMJFS2106].

ORCID

Natsumi Ito http://orcid.org/0009-0008-6765-3395
Ahmed Nabil http://orcid.org/0000-0002-5617-4726
Koichiro Uto http://orcid.org/0000-0001-7091-0585
Mitsuhiro Ebara http://orcid.org/0000-0002-7906-0350

Supporting Information

Supporting information provide ^{1}H-NMR spectrum of samples (Figure S1), Change in absorbance of DPBF (Figure S2), Fluorescence staining with FerroOrange^{TM} (Figure S3), and Cell viability of MCF-7 cells (Figure S4).

References

[1] Gonçalves AC, Richiardone E, Jorge J, et al. Impact of cancer metabolism on therapy resistance - clinical implications. Drug Resist Updat. 2021;59:100797. doi: 10.1016/j.drup.2021.100797
[2] Dai EY, Han L, Liu J, et al. Autophagy-dependent ferroptosis drives tumor-associated macrophage polarization via release and uptake of oncogenic KRAS protein. Autophagy. 2020;16(11):2069–2083. doi: 10.1080/15548627.2020.1714209
[3] Boumahdi S, de Sauvage FJ. The great escape: tumour cell plasticity in resistance to targeted therapy. Nat Rev Drug Discov. 2020;19(1):39–56. doi: 10.1038/s41573-019-0044-1
[4] Han F, Li SJ, Yang YK, et al. Interleukin-6 promotes ferroptosis in bronchial epithelial cells by inducing reactive oxygen species-dependent lipid peroxidation and disrupting iron homeostasis. Bioengineered. 2021;12(1):5279–5288. doi: 10.1080/21655979.2021.1964158
[5] Jung M, Mertens C, Tomat E, et al. Iron as a central player and promising target in cancer progression. Int J Mol Sci. 2019;20(2):273. doi: 10.3390/ijms20020273
[6] Zhao B, Li X, Wang Y, et al. Iron-dependent cell death as executioner of cancer stem cells. J Exp Cli Cancer Res. 2018;37(1):1–3. doi: 10.1186/s13046-018-0733-3

[7] Cosialls E, El Hage R, Dos Santos L, et al. Ferroptosis: cancer stem cells rely on iron until "to die for" it. Cells. 2021;10(11):2981. doi: 10.3390/cells10112981
[8] Dixon SJ, Lemberg KM, Lamprecht MR, et al. Ferroptosis: an iron-dependent form of nonapoptotic cell death. Cell. 2012;149(5):1060–1072. doi: 10.1016/j.cell.2012.03.042
[9] Tang DL, Kang R, Vanden Berghe T, et al. The molecular machinery of regulated cell death. Cell Res. 2019;29(5):347–364. doi: 10.1038/s41422-019-0164-5
[10] Hassannia B, Vandenabeele P, Vanden Berghe T. Targeting ferroptosis to iron out cancer. Cancer Cell. 2019;35(6):830–849. doi: 10.1016/j.ccell.2019.04.002
[11] Nakase I, Gallis B, Takatani-Nakase T, et al. Transferrin receptor-dependent cytotoxicity of artemisinin-transferrin conjugates on prostate cancer cells and induction of apoptosis. Cancer Lett. 2009;274(2):290–298. doi: 10.1016/j.canlet.2008.09.023
[12] Ceci C, Lacal PM, Graziani G. Antibody-drug conjugates: resurgent anticancer agents with multi-targeted therapeutic potential. Pharmacol Ther. 2022;236:108106. doi: 10.1016/j.pharmthera.2021.108106
[13] Tang ZM, Liu YY, He MY, et al. Chemodynamic therapy: tumour microenvironment-mediated Fenton and Fenton-like reactions. Angew Chem Int Ed. 2019;58(4):946–956. doi: 10.1002/anie.201805664
[14] Stoyanovsky DA, Tyurina YY, Shrivastava I, et al. Iron catalysis of lipid peroxidation in ferroptosis: regulated enzymatic or random free radical reaction? Free Radic Biol Med. 2019;133:153–161. doi: 10.1016/j.freeradbiomed.2018.09.008
[15] Efferth T, Benakis A, Romero MR, et al. Enhancement of cytotoxicity of artemisinins toward cancer cells by ferrous iron. Free Radic Biol Med. 2004;37(7):998–1009. doi: 10.1016/j.freeradbiomed.2004.06.023
[16] Markowitsch SD, Schupp P, Lauckner J, et al. Artesunate inhibits growth of sunitinib-resistant renal cell carcinoma cells through cell cycle arrest and induction of ferroptosis. Cancers (Basel). 2020;12(11):3150. doi: 10.3390/cancers12113150
[17] White NJ. Qinghaosu (artemisinin): the price of success. Science. 2008;320(5874):330–334. doi: 10.1126/science.1155165
[18] Robert A, Dechy-Cabaret O, Cazelles J, et al. From mechanistic studies on artemisinin derivatives to new modular antimalarial drugs. Acc Chem Res. 2002;35(3):167–174. doi: 10.1021/ar990164o
[19] Nagasaka Y. Standard textbook of nutritional science. Tokyo, Japan: Kanehara & Co. Ltd; 2002. p. 151–152.
[20] Ganz T, Nemeth E. Hepcidin and iron homeostasis. Biochim Biophys Acta Mol Cell Res. 2012;1823(9):1434–1443. doi: 10.1016/j.bbamcr.2012.01.014
[21] Duc D, Devries PJ, Khanh NX, et al. The pharmacokinetics of a single dose of artemisinin in healthy Vietnamese subjects. Am J Trop Med Hyg. 1994;51(6):785–790. doi: 10.4269/ajtmh.1994.51.785
[22] Ding YX, Wan JX, Zhang ZH, et al. Localized Fe(II)-induced cytotoxic reactive oxygen species generating nanosystem for enhanced anticancer therapy. ACS Appl Mater Interfaces. 2018;10(5):4439–4449. doi: 10.1021/acsami.7b16999
[23] Homma T, Kobayashi S, Fujii J. Induction of ferroptosis by singlet oxygen generated from naphthalene endoperoxide. Biochem Biophys Res Commun. 2019;518(3):519–525. doi: 10.1016/j.bbrc.2019.08.073
[24] Turro NJ, Chow MF. Mechanism of thermolysis of endoperoxides of aromatic-compounds-activation parameters, magnetic-field, and magnetic isotope effects. J Am Chem Soc. 1981;103(24):7218–7224. doi: 10.1021/ja00414a029
[25] Wakagi M, Watanabe J, Takahashi S, et al. Interlaboratory validation study of a singlet oxygen absorption capacity assay method for determining the antioxidant capacities of antioxidant solutions and food extracts. Food Sci Technol Res. 2017;23(3):481–485. doi: 10.3136/fstr.23.481
[26] Flors C, Fryer MJ, Waring J, et al. Imaging the production of singlet oxygen in vivo using a new fluorescent sensor, singlet oxygen sensor green®. J Exp Bot. 2006;57(8):1725–1735. doi: 10.1093/jxb/erj181
[27] Guo SD, Yao XX, Jiang Q, et al. Dihydroartemisinin-loaded magnetic nanoparticles for enhanced chemodynamic therapy. Front Pharmacol. 2020;11:226. doi: 10.3389/fphar.2020.00226
[28] Kanda Y. Investigation of the freely available easy-to-use software 'EZR' for medical statistics. Bone Marrow Transplant. 2013 [cited 2012 Dec 3];48(3):452–458. doi: 10.1038/bmt.2012.244
[29] Di Mascio P, Martinez GR, Miyamoto S, et al. Singlet molecular oxygen reactions with nucleic acids, lipids, and proteins. Chem Rev. 2019;119(3):2043–2086. doi: 10.1021/acs.chemrev.8b00554
[30] Klaper M, Wessig P, Linker T. Base catalysed decomposition of anthracene endoperoxide. Chem Commun. 2016;52(6):1210–1213. doi: 10.1039/c5cc08606j
[31] Wichterle O, Lím D. Hydrophilic gels for biological use. Nature. 1960;185(4706):117–118. doi: 10.1038/185117a0
[32] Ismail HM, Barton V, Phanchana M, et al. Artemisinin activity-based probes identify multiple molecular targets within the asexual stage of the malaria parasites *Plasmodium falciparum* 3D7. Proc Natl Acad Sci USA. 2016;113(8):2080–2085. doi: 10.1073/pnas.1600459113
[33] Shindelman JE, Ortmeyer AE, Sussman HH. Demonstration of the transferrin receptor in human breast cancer tissue. Potential marker for identifying dividing cells. Int J Cancer. 1981;27(3):329–334. doi: 10.1002/ijc.2910270311
[34] Faulk WP, Hsi BL, Stevens PJ. Transferrin and transferrin receptors in carcinoma of the breast. Lancet. 1980;316(8191):390–392. doi: 10.1016/S0140-6736(80)90440-7
[35] Roh JL, Kim EH, Jang H, et al. Nrf2 inhibition reverses the resistance of cisplatin-resistant head and neck cancer cells to artesunate-induced ferroptosis. Redox Biol. 2017;11:254–262. doi: 10.1016/j.redox.2016.12.010